JOURNAL OF GUIDANCE, CONTROL, AND DYNAMICS
Vol. 26, No. 6, November–December 2003

Minimum-Time Orbital Phasing Maneuvers

Christopher D. Hall* and Victor Collazo-Perez†
Virginia Polytechnic Institute and State University, Blacksburg, Virginia 24061

The minimum-time, constant-thrust, orbital phasing maneuver is studied numerically. Nondimensionalization reduces the problem to one where thrust magnitude and phase angle are the only parameters. Extremal solutions are obtained for the entire range of practical values of thrust magnitude and phase angle. Plots of trajectories, thrust-angle profiles, and loci of initial costates are used to identify a near-invariance principle that leads to a variety of conclusions about this class of problems. The types of thrust-angle profiles are shown to fall into at least four types, two of which exist within the region of near-invariance. These two thrust-angle profile types are distinguished by the time-of-flight t_f, and the transition between them takes place for a t_f of approximately one-half of an orbit. The relationship between t_f and the ratio of thrust to phase angle is also shown to be nearly invariant over a wide range of thrust magnitudes.

Introduction

WE investigate a special class of coplanar time-optimal orbital maneuvers in which the spacecraft is controlled to move ahead of or behind its orbit position using a constant thrust whose direction is the control variable. This minimum-time orbital phasing maneuver is conceptually simple, but its solution has some interesting characteristics, including an approximate invariance relating the dimensionless thrust, phase angle, dimensionless time-of-flight, and thrust-angle profile when the maneuver occurs in less than about one orbit.

The minimum-time, constant-thrust, orbit transfer problem is well-established as one of the fundamental problems in control of spacecraft trajectories.[1–3] Most researchers find extremal solutions that solve the first-order, or necessary, conditions, and these solutions are generally known also to be optimal solutions. A recently published procedure is now available for applying second-order conditions[4] but is not discussed further in this paper. Many applications of this problem involve low-thrust propulsion systems where the orbit transfer takes place over a relatively long duration. For example, the minimum-time transfer of a 100-kg spacecraft from low Earth orbit (LEO) to geostationary orbit (GEO) using a 1-N thruster takes about 5 days, as compared with about 5 h for a Hohmann transfer, but the continuous-thrust case would typically use much less propellant. The thrust-angle profile of a continuous-thrust orbit transfer depends on both the thrust magnitude and the size of the orbit transfer. For example, Thorne and Hall[5] showed that there are scenarios involving small orbit changes using low thrust that are similar to large-thrust scenarios with larger orbit changes. In Ref. 6 the effects of thrust magnitude on trajectory behavior were described in some detail.

The development in Refs. 5 and 7 led to the identification of three different regimes of minimum-time, constant-thrust, coplanar orbit transfer scenarios, along with a means of approximating the initial conditions of the Lagrange multipliers required to determine the optimal control history. In an application of these approximations, Marasch and Hall[8] used piecewise time-optimal transfers to investigate the effectiveness of using energy storage during eclipse for low-thrust electric propulsion systems.

In the present paper, we consider the minimum-time orbital phasing maneuver using constant thrust with the thrust angle as the control variable. Specifically, we pose and obtain solutions to the problem of moving a point-mass spacecraft from one point in a given circular orbit to a different point in the same orbit, differing only by a phase angle ϕ. This problem is of course the same as the same-orbit rendezvous problem. However, our motivation is not rendezvous, but rather the formation-establishment and formation-keeping maneuvers associated with formation flying missions.[9,10] We want to compute minimum-time solutions for comparison with nonlinear feedback controllers[11–13] designed to support such missions.

We begin by defining the idealized model and stating the equations of motion. The equations are nondimensionalized so that the dimensionless thrust T and the phase angle ϕ are the only parameters in the problem. We then establish the minimum-time transfer problem, which leads to a two-point boundary value problem requiring the determination of the unknown initial conditions for the Lagrange multipliers or costates. We present some example solutions intended to illustrate a certain near-invariance principle that is found within the various families of solutions for varying thrust and phase angle. Specifically, we show that, for a broad range of T and ϕ, extremal solutions with the same time-of-flight t_f have the same thrust-angle profile and, furthermore, that the relationship between t_f and T/ϕ is nearly thrust independent. This near-invariance is one of the primary points of this communication and should be useful in developing further results relevant to this problem. A series of locus plots for the initial conditions of the costates is used to illustrate the near-invariance, and we identify a transition between large-t_f and small-t_f trajectories.

Model and Equations of Motion

We make the idealized assumptions of a point-mass spacecraft moving in a plane about a spherical primary and being controlled with a constant thrust with variable direction. Figure 1 illustrates the geometry and variables of the problem. The position and velocity at the initial time t_0 correspond to counterclockwise circular motion beginning on the x axis. The initial position of the target orbit is on the same circular orbit, separated from the initial spacecraft position by the phase angle ϕ. The position of the target is indicated with an empty circle. A possible thrust-vector direction is shown, with angle ψ between the inertial x axis and the thrust-vector direction, measured counterclockwise as shown. Additionally, we define the thrust angle relative to the local horizontal as $\bar{\psi} = \psi - \theta - \pi/2$. In the figure, an arbitrary intermediate configuration is shown, after time $t - t_0$. The uncontrolled spacecraft position is shown as a light shaded circle on the circular orbit, whereas the actual spacecraft position is shown as a darker shaded circle removed from the circular

Received 10 October 2002; presented as Paper AAS 03-125 at the AAS/AIAA 13th Space Flight Mechanics Conference, Ponce, PR, 9–13 February 2003; revision received 15 May 2003; accepted for publication 15 May 2003.

*Professor, Aerospace and Ocean Engineering; cdhall@vt.edu. Associate Fellow AIAA.

†Graduate Research Assistant, Aerospace and Ocean Engineering; vcollazo@vt.edu.

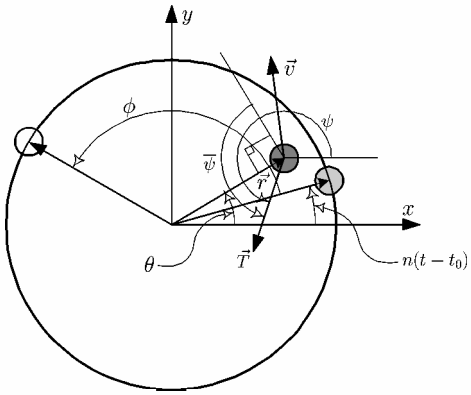

Fig. 1 Optimal phasing maneuver geometry.

orbit. The target position and the uncontrolled spacecraft position have both advanced through an angle $n(t-t_0)$, where n is the mean motion of the circular orbit. If we use polar coordinates, the distinction between ψ and $\bar{\psi}$ can be eliminated; however, we choose to use Cartesian coordinates to simplify the extension of this work to three-dimensional cases.

The equations of motion are those for Keplerian motion in the plane, with additional acceleration terms due to the thruster. We assume the spacecraft has constant mass for the results presented in the paper, and the results are qualitatively unchanged for small $\dot{m}$. Using Cartesian coordinates in the inertial reference frame shown in Fig. 1, the equations of motion are

$$\dot{x}^* = v_x^* \tag{1}$$

$$\dot{y}^* = v_y^* \tag{2}$$

$$\dot{v}_x^* = -(\mu^*/r^{*3})x^* + (T^*/m^*)\cos\psi \tag{3}$$

$$\dot{v}_y^* = -(\mu^*/r^{*3})y^* + (T^*/m^*)\sin\psi \tag{4}$$

where x^* and y^* are the components of the position vector in the orbital plane, $r^* = \sqrt{(x^{*2} + y^{*2})}$, μ^* is the gravitational parameter, ψ is the thrust angle measured from an inertial x axis, T^* is the applied thrust, and m^* is the spacecraft mass. The superscript $*$ denotes that these are dimensional variables. Using dimensional variables requires that we consider the effects of varying orbit size, thrust magnitude, and spacecraft mass; nondimensionalizing the equations reduces the problem to one with only dimensionless thrust as a parameter.

Nondimensionalization is based on canonical units,[14] so that the reference orbit semimajor axis is 1 distance unit (DU), the reference orbit period is 2π time units (TU), and the gravitational parameter is $\mu = 1$ DU^3/TU^2. The spacecraft mass m^* is taken as the dimensionless mass unit, and it follows that a dimensionless thrust can be defined by

$$T = \frac{T^*}{m^* a^* n^{*2}} \tag{5}$$

where a^* is the reference orbit semimajor axis and n^* is the reference mean motion in dimensional units. Thus, for example, a 1-N thruster acting on a 100-kg spacecraft in a 10,000-km-radius circular orbit provides a dimensionless thrust of about $T = 0.0025$. In results illustrated below, we use the range [0.000005, 0.5] as a practical limit on the range of thrusts of interest for this application. For a 100-kg spacecraft, this range corresponds to approximately [4 mN, 400 N] in LEO and [100 μN, 10 N] in GEO. Even smaller thrusts may be of interest, but the near-invariance described later can be used to obtain results for smaller thrusts in a straightforward way. The expression for T can also be written as

$$T = \frac{(T^*/m^*)}{(\mu^*/a^{*2})} \tag{6}$$

so that T can be interpreted as the ratio of thrust acceleration to gravitational acceleration.

The form of the dimensionless equations is identical to that of the dimensional equations, with the asterisks omitted, and both μ and m set to unity. Thus, the dimensionless states are (x, y, v_x, v_y), and the only parameter remaining in the equations of motion is the dimensionless thrust magnitude T. The other nonstate variable in the equations of motion is the thrust angle ψ, which is the control variable to be determined.

Optimal Control Formulation and Boundary Value Problem

The minimum-time formulation is well known and may be found, for example, in Refs. 1, 2, 3, and 5. The formulation leads to four additional differential equations describing variables variously known as costates or Lagrange multipliers. These four differential equations are

$$\dot{\lambda}_x = \lambda_{v_x}/r^3 - (3x/r^5)\left(x\lambda_{v_x} + y\lambda_{v_y}\right) \tag{7}$$

$$\dot{\lambda}_y = \lambda_{v_y}/r^3 - (3y/r^5)\left(x\lambda_{v_x} + y\lambda_{v_y}\right) \tag{8}$$

$$\dot{\lambda}_{v_x} = -\lambda_x \tag{9}$$

$$\dot{\lambda}_{v_y} = -\lambda_y \tag{10}$$

and they are to be integrated simultaneously with the state equations (1–4). Note that we have made use of the fact that $\mu = 1$ in the dimensionless system.

The thrust angle is found from the optimal control formulation to be

$$\psi = \tan^{-1}\left(-\lambda_{v_y}/-\lambda_{v_x}\right) \tag{11}$$

and this angle is used as the control in Eqs. (3) and (4).

In a typical scenario, we know the initial conditions on the states and at least something about the final conditions on the states. However, we do not know the initial or final conditions on the costates. Thus, we establish a two-point boundary value problem wherein the initial conditions on the costates are the unknowns.

For the phasing maneuver considered here, the initial conditions for the states are $x = 1$, $y = 0$, $v_x = 0$, and $v_y = 1$, corresponding to a circular orbit with radius 1 DU beginning on the x axis. The final conditions that the states must satisfy include that the spacecraft must return to the same circular orbit; that is, $x^2 + y^2 = 1$, $v_x^2 + v_y^2 = 1$, and $xv_x + yv_y = 0$. In addition to these three conditions, we also have the condition corresponding to completion of the phasing maneuver through angle ϕ. Another way to formulate the final conditions on the states is

$$x(t_f) = \cos(\phi + t_f) \tag{12}$$

$$y(t_f) = \sin(\phi + t_f) \tag{13}$$

$$v_x(t_f) = -\sin(\phi + t_f) \tag{14}$$

$$v_y(t_f) = \cos(\phi + t_f) \tag{15}$$

where t_f is the time of flight, which is also unknown. An added benefit of the nondimensionalization is that t_f is the angle the target moves through during the maneuver.

Because the variational Hamiltonian is linear in the Lagrange multipliers, we can arbitrarily fix the initial condition of one of the multipliers,[5] and we select $\lambda_x(0) = \pm 1$. The choice of $\lambda_x(0) = +1$ leads to the correct solution for the case where $0 < \phi < \pi$, whereas $\lambda_x(0) = -1$ provides the correct solution for the case where $-\pi < \phi < 0$. This skew symmetry in the structure of solutions is described in more detail in the following.

Thus, the unknowns in the boundary value problem are $\lambda_y(0)$, $\lambda_{v_x}(0)$, $\lambda_{v_y}(0)$, and t_f, and so the problem may be stated as

$$F\left(\lambda_y(0), \lambda_{v_x}(0), \lambda_{v_y}(0), t_f\right) = \begin{bmatrix} x(t_f) - \cos(\phi + t_f) \\ y(t_f) - \sin(\phi + t_f) \\ v_x(t_f) + \sin(\phi + t_f) \\ v_y(t_f) - \cos(\phi + t_f) \end{bmatrix} = 0 \quad (16)$$

where T is a fixed constant appearing in the equations of motion, which are numerically integrated from $t = 0$ to $t = t_f$ to compute the final states, and ϕ is a fixed constant appearing in the final-time boundary conditions. This problem can be solved using Newton's method or another appropriate numerical method.[15] All solutions presented in this paper were computed using Matlab's fsolve function with a tolerance setting of 10^{-11}. The stringent accuracy was used to ensure stability in the continuation approach[16] used to obtain solutions for many combinations of T and ϕ.

Example Solutions

In this section we present four examples of minimum-time trajectories. The examples illustrate the nature of solutions to the optimal control problem with varying thrust T and phase angle ϕ. For each example we provide plots of the trajectory and the thrust angle relative to the local horizontal. As noted in the preceding section, all trajectories begin with initial conditions $x = 1$, $y = 0$, $v_x = 0$, and $v_y = 1$. In Table 1, we provide the parameters (T, ϕ) for each case, as well as some data specific to the solution for each case.

The first example illustrates a maneuver through a small phase angle, $\phi = 0.21$, using a large thrust, $T = 0.05$ (Figs. 2a and 2b). The trajectory (solid line) and the circular orbit (dashed line) are both shown in Fig. 2a, where it is evident that the trajectory is completed in just over one-half of an orbital period ($t_f \approx 4$). Figure 2a also includes a sequence of line segments indicating the thrust direction along the trajectory. Of the four costates, only the pair $(\lambda_{v_x}, \lambda_{v_y})$ is used in computing the thrust angle ψ, using Eq. (11). Although the angle ψ is useful in solving the boundary value problem and in plotting the thrust direction as in Fig. 2a, it is not particularly useful to plot the angle itself because of its interaction with the spacecraft's position in the inertial frame. Therefore, we plot the thrust angle referenced to the local horizontal, denoted by $\bar{\psi}$, as indicated in Fig. 1. The thrust-angle history is shown in Fig. 2b. Note that the initial thrust angle is in the second quadrant, which has the effect of lowering the orbit, thereby increasing the orbital speed so that the spacecraft catches up with the target. At about the halfway point, the thrust vector switches direction so that the orbit is raised to achieve the rendezvous. The thrust-angle profile is easily seen in both Figs. 2a and 2b.

Case 2 illustrates a small-phase-angle maneuver using a small thrust (Figs. 2c and 2d). This case is interesting because of its similarity to case 1, even though the (T, ϕ) parameters differ by four orders of magnitude: (0.05, 0.21) vs (0.000005, 0.000022). The two trajectories shown in Figs. 2a and 2c are similar in that the thrust-angle profiles and times of flight are nearly the same, although the lower thrust in case 2 leads to a smaller change in radius during the maneuver. Note the similarities between the thrust-angle histories, as seen in Figs. 2b and 2d. The costate histories (not shown here) exhibit the same equivalence. In both cases, the thrust begins in a rearward, inward direction and swings through $\bar{\psi} = 0$ at about the

Table 1 Four example cases

Case no.	T	ϕ	$\lambda_{v_x}(0)$	$\lambda_{v_y}(0)$	t_f
1	0.05	0.2101	0.6906	0.5000	3.6599
2	0.00005	0.00002246	0.5548	0.5000	3.8195
3	0.05	3.0	0.4531	0.8745	8.7342
4	0.00005	0.3	0.0113	0.9960	89.3266

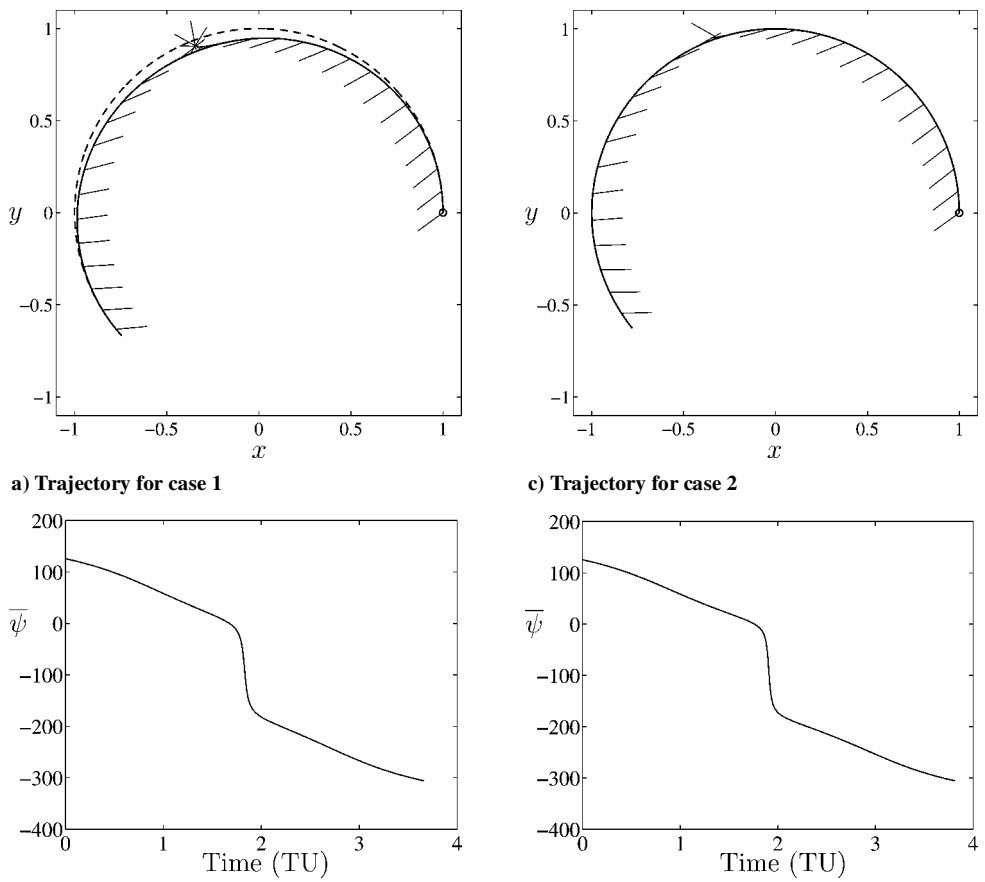

a) Trajectory for case 1

c) Trajectory for case 2

b) Thrust angle for case 1

d) Thrust angle for case 2

Fig. 2 Trajectory and thrust angle for cases 1 ($T = 0.05$, $\phi = 0.21$) and 2 ($T = 0.000005$, $\phi = 0.000022$).

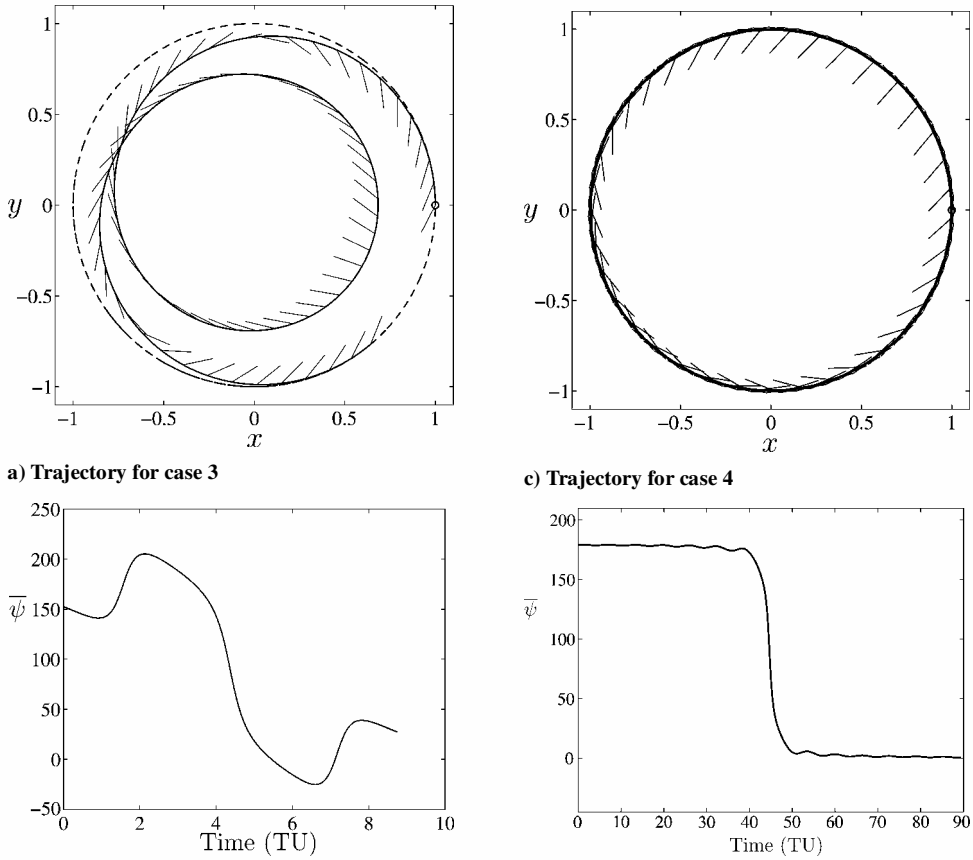

Fig. 3 Trajectory and thrust angle for cases 3 (T = 0.05, ϕ = 3.0) and 4 (T = 0.00005, ϕ = 0.3).

midway point and, thus, includes a brief period of outward thrusting. The similarities between cases 1 and 2 are evident in many other cases and we develop this idea further in the remainder of the paper.

The third case displays quite different behavior from cases 1 and 2 (Figs. 3a and 3b). Case 3 uses the same thrust as in case 1 ($T = 0.05$), but the maneuver is through a larger phase angle ($\phi = 3.0$). The maneuver takes almost two orbits. Figure 3b illustrates the thrust-angle profile for this maneuver, which exhibits an interesting "porpoising" behavior.

The final case illustrated in full is case 4, where a relatively large phase-angle maneuver, $\phi = 0.3$, is effected using a small thrust, $T = 0.00005$ (Figs. 3c and 3d). Here the thrust is nearly tangential throughout the maneuver, with the first half of the maneuver using orbit-lowering to catch up with the target and the second half raising the orbit with a nearly tangential thrust in the velocity direction. The thrust vectors shown in Fig. 3c appear to be mostly inward, but this misperception is because most of the thrusting is tangential, except for the period of roughly 10 TUs (about 1.5 orbits) at the halfway point where the thrust changes directions, as seen more readily in Fig. 3d. The tangential thrust vectors do not show up in Fig. 3c because they overlap the trajectory. This maneuver takes about 15 orbits to complete.

The four example cases presented in Figs. 2 and 3 and Table 1 are intended to illustrate the near-invariance that is discussed in more detail in the following, as well as to illustrate the different types of trajectories that may occur for this problem. There are four basic types of trajectories that occur as extremal solutions to the minimum-time phasing maneuver, three of which are illustrated in these four cases: 1) initial inward, rearward thrusting with a swing through $\bar{\psi} = 0$ near the trajectory midpoint, as in cases 1 and 2; 2) multiple-revolution trajectories with thrust angle $\bar{\psi}$ passing through zero multiple times, as in case 3; and 3) multiple-revolution trajectories with thrust angle $\bar{\psi}$ rearward tangential for most of the maneuver, with a swing through $\bar{\psi} = 90$ deg near the midpoint and forward tangential thrusting for the remainder of the trajectory, as in case 4. The fourth type of trajectory is illustrated in a subsequent section.

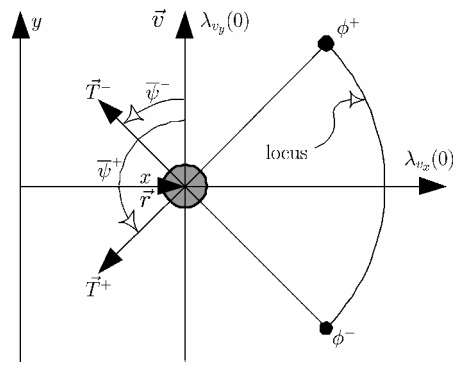

Fig. 4 Example locus of costates illustrating thrust angle.

Locus of Costate Initial Conditions

Once a solution for a given (T, ϕ) pair has been obtained, we obtain solutions for additional cases using numerical continuation.[16] Many thousands of solutions are obtained, and convergence is sensitive to small changes in the initial guess; thus, continuation provides a robust approach to compute additional solutions while varying parameters. As an example, we illustrate a locus of the initial conditions of (λ_{v_x}, λ_{v_y}) in Fig. 4. The diagram shows how the initial costate locus can be interpreted as the initial thrust angle. That is, we juxtapose the costate locus and the Cartesian coordinate frame so that the origin of the locus coincides with the initial spacecraft position. Then the vector from the initial costate to the spacecraft position defines the initial thrust-vector direction. Initial costates with $\lambda_{v_y} > 0$ correspond to initially thrusting inward and rearward,

whereas $\lambda_{v_y} < 0$ corresponds to initially thrusting inward and forward. In the diagram we show a segment of a typical locus plot, for a fixed thrust T, with ϕ varying on the interval $[\phi^-, \phi^+]$. For the two endpoints, we show how to construct the initial thrust vectors $\boldsymbol{T}^-$ and $\boldsymbol{T}^+$ and the associated initial thrust angles $\bar{\psi}^-(0)$ and $\bar{\psi}^+(0)$. Obviously, since $\phi^+ > \phi^-$, one expects the t_f for ϕ^+ to be greater than that for ϕ^-, which is indeed the case. Thus, as one moves from ϕ^- to ϕ^+ along the locus, t_f increases and, at least for the range shown, $\bar{\psi}(0)$ increases. Each point on the locus corresponds to a specific initial thrust angle, as well as to a specific time of flight t_f. Thus, we can identify each point on the locus with the following mapping:

$$(T, \phi) \mapsto (\lambda_{v_x}, \lambda_{v_y}, \psi, t_f) \tag{17}$$

We present a set of locus plots illustrating the entire range of reasonable values of (T, ϕ) and develop the near-invariance that arises in the mapping defined by Eq. (17).

We also note the skew symmetry in the costate locus related to the sign of the phase angle. If $\phi \in (0, \pi)$, then the locus of initial costates is in the right half of the $(\lambda_{v_x}, \lambda_{v_y})$ plane, and the choice of $\lambda_x(0) = 1$ [as described following Eqs. (12–15)] is correct. If $\phi \in (-\pi, 0)$, then the locus of initial costates is in the left half of the plane, and the choice $\lambda_x(0) = -1$ is correct. Furthermore, $\phi \mapsto -\phi$ (within these ranges) corresponds to $(\lambda_{v_x}, \lambda_{v_y}) \mapsto (-\lambda_{v_x}, -\lambda_{v_y})$.

We use continuation to obtain solutions for $\phi \in (0, \pi)$ and $T \in [0.000005, 0.5]$ and use the results to construct locus plots of the initial conditions of $(\lambda_{v_x}, \lambda_{v_y})$. Note that, for smaller values of T, we do not obtain solutions for larger values of ϕ because of the extreme times of flight required, and, for larger values of T, we do not obtain solutions for smaller values of ϕ because of the extreme sensitivity. We also do not compute solutions for $\phi > \pi$ because one would normally choose the short-way solution, taking advantage of the skew-symmetry of the costate locus described earlier.

Figure 5 presents the locus of initial costates for $T \in [0.000005, 0.05]$ and $\phi \in (0, \pi)$. In each of these graphs, the initial values of $(\lambda_{v_x}, \lambda_{v_y})$ are plotted for a fixed value of T while varying the phase angle ϕ. Beginning in the lower half of one of these graphs [in the vicinity of $(0, -1)$] corresponds to a small phase angle, and the end of the graph [in the vicinity of the point $(0, 1)$] corresponds to the largest value of ϕ for that graph. For the larger thrust values ($T \geq 0.005$), the endpoint corresponds to $\phi = \pi$, whereas for the smaller thrust values, the endpoint corresponds to $\phi < \pi$. For example, for $T = 0.0005$, the endpoint in the graph is for $\phi = 2.25$, and the corresponding trajectory has a time of flight of 77 TUs (about 12 orbits). The points labeled A, B, C, and D in the locus plots are described in detail later, and correspond to the data in Table 2.

As described earlier, one can view each point on each of these graphs as corresponding to a specific thrust and phase angle, (T, ϕ), to a specific costate history $\lambda(t)$, and to a specific time of flight, t_f. Several properties of the costate loci that are presented in Fig. 5 are of interest:

1) Each locus begins near the point $(0, -1)$ corresponding to tangential thrust in the direction of the velocity vector. This observation is consistent with the idea that using a large thrust to effect a small phase-angle change would begin the maneuver by thrusting toward the destination, then switching thrust direction to decelerate to the desired state. This observation is true for small T as well, but corresponds to a smaller phase angle than in the large-T cases. We refer to this region of the locus as the small-t_f region; generally, increasing thrust or decreasing the phase angle corresponds to decreasing t_f and moving along the locus toward $(0, -1)$.

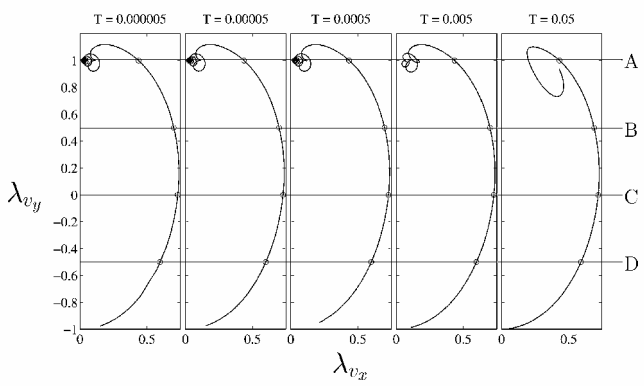

Fig. 5 Locus of costates for $T \in [0.000005, 0.05]$, $\phi \in (0, \pi)$.

Table 2 Data for specific points on the locus plots

Point	T	ϕ	$\lambda_y(0)$	$\lambda_{v_x}(0)$	$\lambda_{v_y}(0)$	t_f
A	0.5	——	——	——	——	——
	0.05	0.89	0.34	0.43	1.0	5.6
	0.005	0.10	0.33	0.44	1.0	6.2
	0.0005	0.010	0.33	0.44	1.0	6.3
	0.00005	0.0010	0.33	0.44	1.0	6.3
	0.000005	0.00010	0.33	0.44	1.0	6.3
B	0.5	1.46	0.47	0.63	0.5	2.8
	0.05	0.21	0.44	0.69	0.5	3.7
	0.005	0.022	0.44	0.70	0.5	3.8
	0.0005	0.0022	0.44	0.70	0.5	3.8
	0.00005	0.00022	0.44	0.70	0.5	3.8
	0.000005	0.000022	0.44	0.70	0.5	3.8
C	0.5	0.54	0.14	0.67	0.0	2.0
	0.05	0.071	0.18	0.73	0.0	2.4
	0.005	0.0074	0.18	0.73	0.0	2.4
	0.0005	0.00074	0.19	0.73	0.0	2.4
	0.00005	0.000074	0.19	0.73	0.0	2.4
	0.000005	0.0000074	0.19	0.73	0.0	2.4
D	0.5	0.17	−0.75	0.53	−0.5	1.2
	0.05	0.022	−0.61	0.60	−0.5	1.4
	0.005	0.0023	−0.60	0.60	−0.5	1.4
	0.0005	0.00023	−0.59	0.60	−0.5	1.4
	0.00005	0.000023	−0.59	0.60	−0.5	1.4
	0.000005	0.0000023	−0.59	0.60	−0.5	1.4

2) Each locus passes close to the point $(0.73, 0)$, corresponding to thrust in the nadir direction. This point can be thought of as a transition point between the typical small-t_f and large-t_f scenarios. We refer to this region of the locus as the transition region; here the time of flight is about one-half of an orbit. A more precise transition point is identified in subsequent text.

3) Each locus moves in a looping pattern toward the point $(0, 1)$ corresponding to tangential thrust in the direction opposite the velocity vector. This observation is consistent with the idea that using a small thrust to effect a large phase-angle change would begin the maneuver by thrusting backward to lower the orbit and catch up with the target. We refer to this region as the large-t_f region; generally, decreasing T or increasing ϕ leads to an increase in t_f and initial costates closer to the point $(0, 1)$.

4) The locus graphs are nearly identical in the lower-phase-angle portions of the graphs before the looping pattern begins. For smaller values of thrust, the locus plots are indistinguishable except in the fine structure of the loops near $(0, 1)$.

5) Not immediately evident in the graphs, but supported by the data in Table 2 and by subsequent plots, is the fact that the thrust-angle profile and time of flight for a point in one of the locus plots is nearly identical to the thrust-angle profiles and times of flight for the corresponding points on the other locus plots.

These properties of the locus graphs can be used to draw some more general conclusions about the minimum-time trajectories. In the next section, we develop the near-invariance principle using these locus graphs.

Discussion of the Near-Invariance

The near-invariance is most valid for small thrust, and so in the discussion that follows we omit the $T = 0.5$ case. However, one can easily refer to Table 2 to compare the $T = 0.5$ case to the rest of the cases that are described in more detail.

On each of the locus graphs, we indicate four points, labeled A, B, C, and D, that share the same initial values of λ_{v_y}. That is, the points labeled A all have $\lambda_{v_y} = 1.0$, and so forth, as detailed in Table 2. These points are of interest because they help to illustrate the

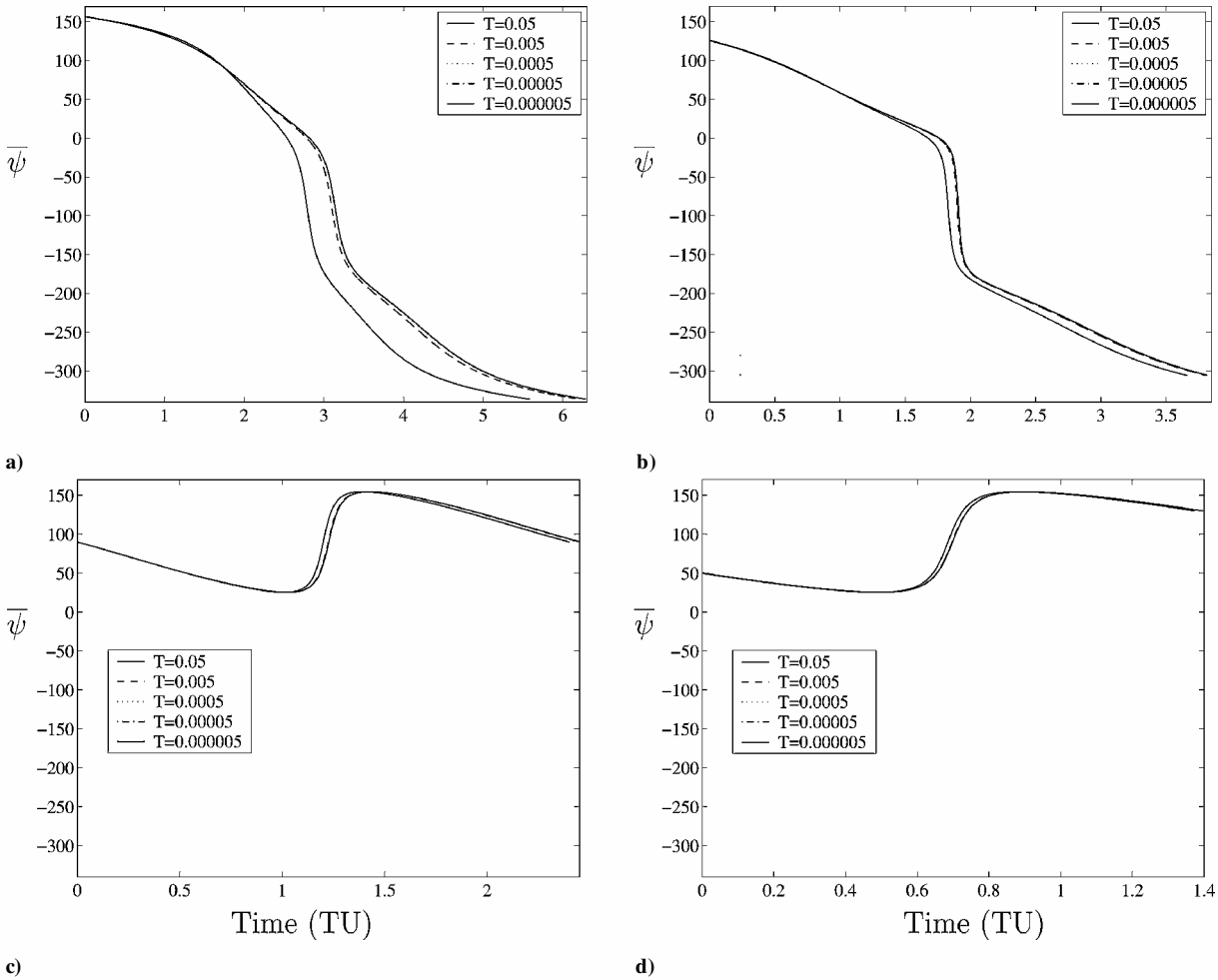

Fig. 6 Thrust angle $\bar{\psi}$ for points A, B, C, and D.

near-invariance that we wish to emphasize. Because the invariance is least accurate in the large-t_f region, we begin by discussing the points A on the composite locus graph in Fig. 5.

In the rightmost graph of Fig. 5, the point A, selected for $\lambda_{v_y}(0) = 1$, corresponds to $(T, \phi) = (0.05, 0.89)$. The initial costates are given in Table 2 along with t_f, which is approximately 5.6, corresponding to completing the maneuver in a little less than one orbit ($t_f = 2\pi$ corresponds to a one-orbit transfer). There is no corresponding point for $T = 0.5$ in Table 2 because for this large value of thrust, the time it takes to reach $\phi = \pi$ is less than for the smaller thrust cases; in fact, if one continues the locus for $\phi > \pi$, the locus loops never reach $\lambda_{v_y} = 1$. In Fig. 5, the thrust in the $T = 0.005$ graph is one order of magnitude smaller (by design), as is the phase angle ($0.89 \approx 10 \times 0.10$, by observation), and the solution has similar values for the other two initial costates and for the time of flight ($5.6 \approx 6.2$). For $T = 0.0005$, the phase angle corresponding to point A is one order of magnitude smaller than for $T = 0.005$, with two significant digits of agreement, and the time of flight is identical to two significant digits. This trend continues for the two smaller values of thrust, with the additional costates and time of flight agreeing exactly to within two significant digits, and the phase angle decreasing by the same order of magnitude as T. Note that we include only two significant digits in Table 2 specifically to highlight the near-invariance. We compute all solutions with a convergence tolerance of 10^{-11}; however, the data presented in the table are sufficient to achieve convergence in about four iterations in most cases. As thrust decreases, the near-invariance becomes more pronounced, and as thrust increases, the near-invariance becomes less significant. However, the time of flight for all five values of thrust is in agreement to one significant digit and, for the three smaller values of thrust, $t_f = 6.3$ to two significant digits. For points B, C, and D, the near-invariance is even more pronounced.

Because the initial costates are nearly the same for all the points labeled A, the initial thrust angle is also nearly the same for all of these points. Furthermore, the thrust-angle profiles for the entire maneuver are nearly the same for all five points. The thrust-angle profiles $\bar{\psi}(t)$ are illustrated in Fig. 6 along with those for points B, C, and D. In the figure, the initial values $\bar{\psi}(0)$ are all essentially identical, and although the thrust-angle profiles are not all identical, they are quite similar. The high-thrust case, $T = 0.05$, produces the profile that differs most from the others, with a significant difference near the midpoint, and with a shorter time of flight. However, the other four cases lead to almost identical thrust-angle profiles for the entire maneuver, in spite of the orders-of-magnitude difference between the thrust values. These observations are increasingly true for the smaller times of flight for points B, C, and D.

The points labeled B in Fig. 5 are chosen for $\lambda_{v_y} = 0.5$. As shown in Table 2, $T \propto \phi$ for all five values of T. The thrust-angle profiles are shown in Fig. 6. The thrust angle $\bar{\psi}$ begins as an inward, backward thrust, and the angle decreases, passing through zero and swinging around through 360 deg to end with an inward, forward thrust. These thrust-angle profiles are similar to those of points A and include the two thrust-angle profiles of cases 1 and 2 illustrated in Fig. 2. These thrust-angle profiles are characteristic of a subset of the large-t_f set of trajectories. The near-invariance of the thrust-angle profile and time of flight is more noticeable for points B than for points A. The maneuvers all take a little more than half an orbit.

The points labeled C are chosen for $\lambda_{v_y} = 0$, which corresponds to initial thrust in the nadir direction. Again, $T \propto \phi$ is evident from the data in Table 2. The thrust-angle profiles, shown in Fig. 6, are substantially different from those of points A and B. The initial thrust is in the nadir direction, and the thrust angle initially decreases but does not pass through zero as in the large-t_f cases. Rather $\bar{\psi}$ reaches a minimum of about 25 deg, then rapidly increases to about

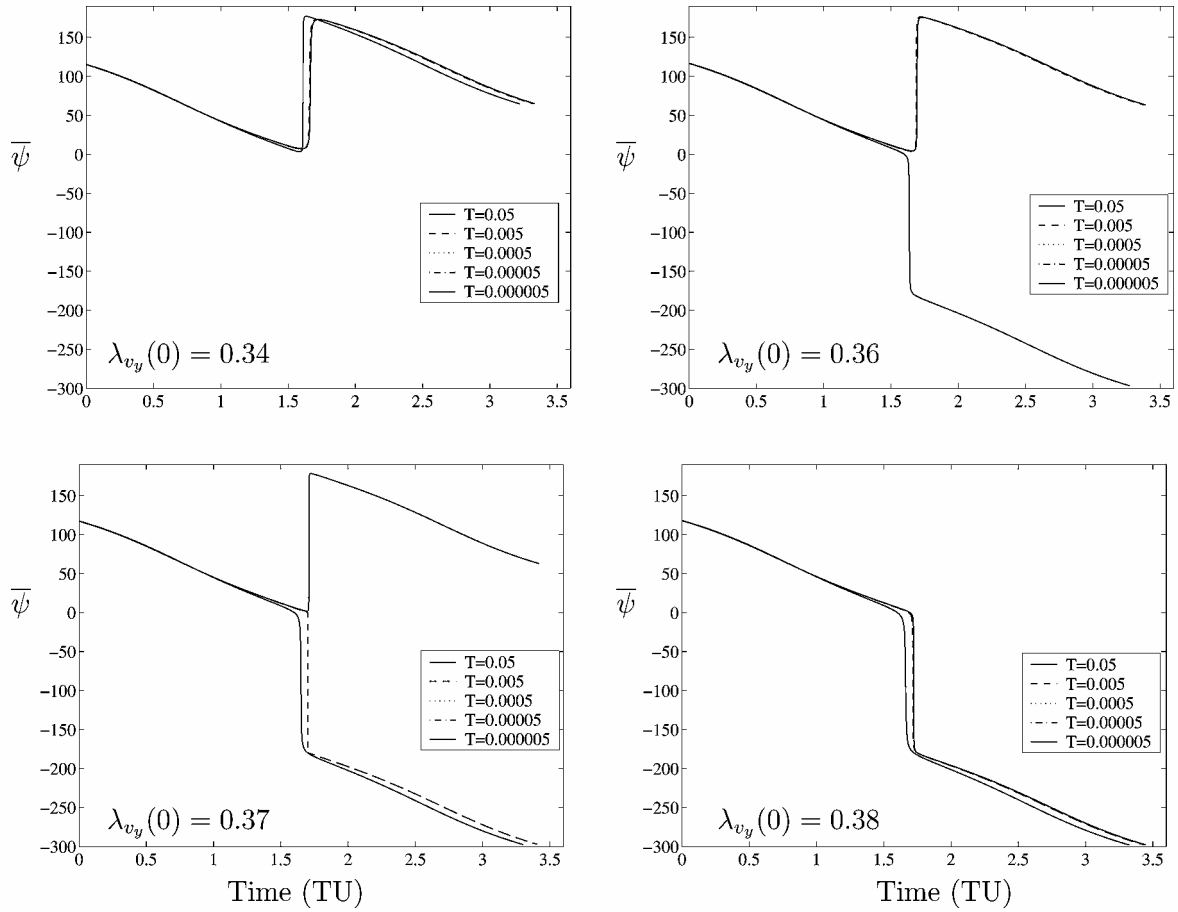

Fig. 7 Thrust angle $\bar{\psi}$ for points with $\lambda_{v_y}(0) \in \{0.34, 0.36, 0.37, 0.38\}$.

155 deg before decreasing again to its final value of about 90 deg. These thrust-angle profiles are characteristic of all of the small-t_f trajectories. Furthermore, for some point between B and C, there is a transition between the large-t_f– and small-t_f–type trajectories, and we subsequently identify this transition behavior.

The points labeled D are chosen for $\lambda_{v_y} = -0.5$, which corresponds to initial thrust in an inward, forward direction. The linear relationship between T and ϕ is evident from the data in Table 2. The thrust-angle profiles, shown in Fig. 6, are similar to those for points C. These maneuvers all take about a quarter orbit to complete.

Comparing the thrust-angle profiles associated with points A and B (large t_f) with those of points C and D (small t_f), it appears that a transition point exists between the two types of profiles. Using bisection, we find that the transition between small-t_f and large-t_f trajectories occurs for $t_f \approx 3.3$. Figure 7 illustrates the thrust-angle profiles for points along the locus with $\lambda_{v_y}(0) \in \{0.34, 0.36, 0.37, 0.38\}$, showing that the transition occurs for slightly different values of t_f for the different values of thrust. All four plots use the same limits to clarify the differences and similarities between the two types of profiles. In particular, note that, except for the direction of the 180-deg swing that occurs in each type of solution, the thrust-angle profiles are essentially identical. In principle, we could add a line in Fig. 5 at $\lambda_{v_y} \approx 0.37$ to indicate this transition family of trajectories.

The final observation we make is to characterize the t_f invariance that has been described. In Fig. 8, we plot curves of constant t_f in the (T, ϕ) plane, with $T \in (5 \times 10^{-6}, 4)$ and $\phi \in (0, 2\pi)$. The thin lines represent solutions for $t_f \in \{\pi/2, \pi, 3\pi/2, \ldots, 4\pi\}$. The thick lines use the four values of t_f associated with $T = 0.000005$ for points A, B, C, and D, and the specific A, B, C, and D points are identified on the plot. Even though the plot is a log–log plot, the linearity of T vs ϕ is remarkable, even across the small-t_f–large-t_f transition. Only in the large-T–large-ϕ region does the linearity

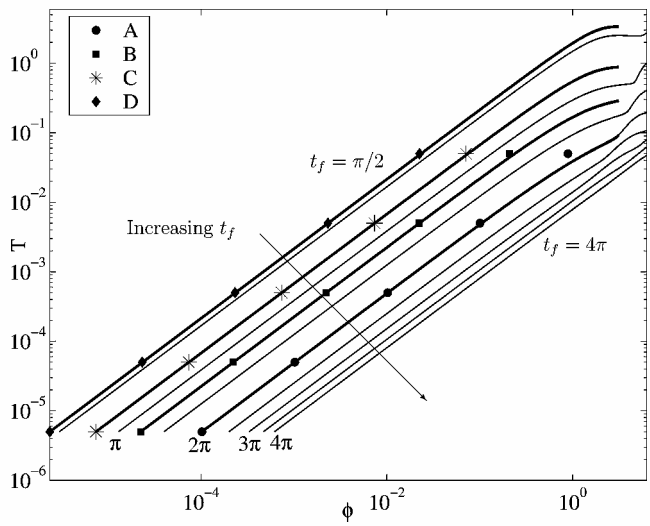

Fig. 8 Constant t_f curves in (T, ϕ) plane.

begin to break down. The A, B, C, and D points clearly lie along the constant t_f curves for most of the points shown. The curves are nearly linear until ϕ approaches π, and there are some interesting variations in the $\phi > \pi$ region, especially for larger thrust. We do not investigate these $\phi > \pi$ cases further, as one would normally use the $\phi - 2\pi$ trajectory and the skew symmetry described earlier in this paper.

We further characterize the relationship between T, ϕ, and t_f by plotting t_f vs T/ϕ for the full range of these parameters presented in earlier plots and tables. The plot in Fig. 9 is a log–log plot of the time

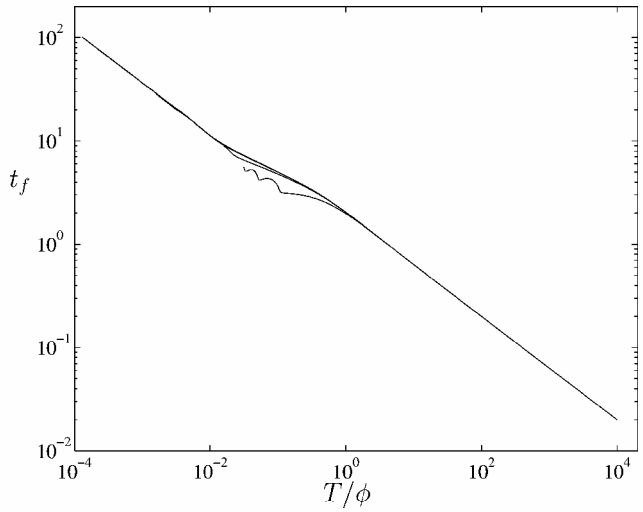

Fig. 9 Relationship between t_f and T/ϕ.

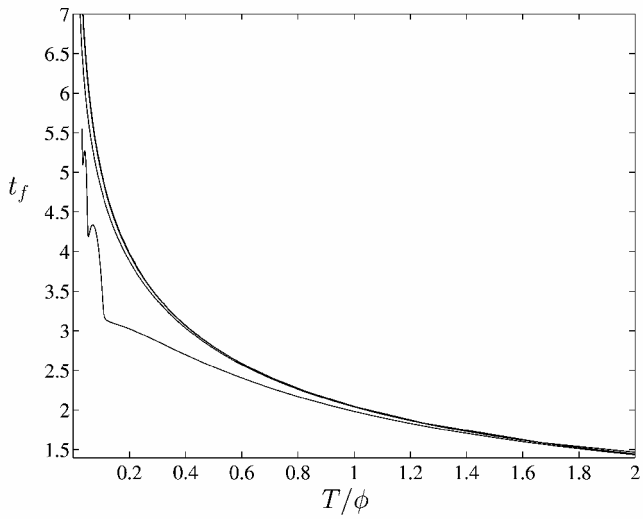

Fig. 10 Relationship between t_f and T/ϕ in transition region.

of flight vs the ratio of thrust to phase angle for each of the different values of thrust (including $T = 0.5$). The thrust-to-phase-angle ratio ranges between 10^{-4} and 10^4, with resulting times of flight ranging between 10^{-2} and 10^2. For most of this range, the graphs are linear and are essentially identical for all the values of thrust. However, in the region where $T/\phi \in (0.01, 1)$, there is a nonlinear transition, which is simple for most of the values of T; for large T (0.5), however, the graph exhibits a more complicated behavior. In Fig. 10, we plot t_f vs T/ϕ on a linear graph in the range $T/\phi \in [0, 2]$, which corresponds to the range where the nonlinear transition is evident in Fig. 9. The complicated relationship between t_f and T/ϕ for $T = 0.5$ is evident here, whereas the relationship between t_f and T/ϕ is quite simple for the smaller values of T, which includes essentially all values of T of interest. Note that the transitional region in Figs. 9 and 10, where the plots of t_f vs T/ϕ are not nearly identical, begins near the transition time of flight, $t_f \approx 3.3$, identified in Fig. 7. The relationship between t_f and T/ϕ can be used for mission planning by permitting the analyst to obtain a quick estimate of the time of flight for a given scenario and propulsion system and thereby obtain a quick estimate for the fuel required for a minimum-time phasing maneuver.

Finally, we note that the invariance illustrated here could be interpreted as simply the linearity associated with small perturbations from the desired position, and indeed we expect that a careful comparison with solutions of the linearized equations of motion would provide consistent results in the same regions where the near-invariance occurs. However, the fact that these results are obtained from the nonlinear equations of motion with a broad range of thrust and phase angles provides a deeper insight into this entire class of orbit transfers.

Conclusions

The extremal solutions to the minimum-time, constant-thrust phasing maneuver problem have some interesting properties that have not previously been reported. Using the equations of motion in a dimensionless form permits the investigation of essentially all problems of interest in one setting, with dimensionless thrust T and phase angle ϕ as the only parameters. The initial costates have a uniform structure that can be exploited when seeking solutions for problems with a specific thrust and phase. There is a near-invariance property that relates the dimensionless time of flight t_f to the thrust and phase: for a wide range of parameter values, a nearly linear relationship exists between the thrust and phase for a given time of flight. This relationship persists even in the transition region that distinguishes maneuvers with only inward thrusting from those with some outward thrusting. The results presented here provide a thorough foundation for future studies of continuous-thrust problems of this type.

Acknowledgments

This work was supported by Arje Nachman of the Air Force Office of Scientific Research and by David Folta of NASA Goddard Space Flight Center. The authors are grateful to Eugene Cliff, Fred Lutze, and Bo Naasz of the Department of Aerospace and Ocean Engineering at Virginia Polytechnic Institute and State University for many useful discussions regarding this problem.

References

[1] Lawden, D. F., *Optimal Trajectories for Space Navigation*, Butterworths, London, 1963, Chap. 6.

[2] Bryson, A. E., Jr., and Ho, Y.-C., *Applied Optimal Control: Optimization, Estimation, and Control*, Wiley, New York, 1975, pp. 66–69.

[3] Marec, J. P., *Optimal Space Trajectories*, Studies in Astronautics, Vol. 1, Elsevier, Amsterdam, 1979.

[4] Jo, J.-W., and Prussing, J. E., "Procedure for Applying Second-Order Conditions in Optimal Control Problems," *Journal of Guidance, Control, and Dynamics*, Vol. 23, No. 2, 2000, pp. 241–250.

[5] Thorne, J. D., and Hall, C. D., "Minimum-Time Continuous-Thrust Orbit Transfers," *Journal of the Astronautical Sciences*, Vol. 45, No. 4, 1997, pp. 411–432.

[6] Alfano, S., and Thorne, J. D., "Constant-Thrust Orbit-Raising," *Journal of Astronautical Sciences*, Vol. 42, No. 1, 1994, pp. 35–45.

[7] Thorne, J. D., and Hall, C. D., "Approximate Initial Lagrange Costates for Continuous Thrust Spacecraft," *Journal of Guidance, Control, and Dynamics*, Vol. 19, No. 2, 1996, pp. 283–288.

[8] Marasch, M. W., and Hall, C. D., "Application of Energy Storage to Solar Electric Propulsion Orbital Transfer," *Journal of Spacecraft and Rockets*, Vol. 37, No. 5, 2000, pp. 645–653.

[9] Hughes, S. P., and Hall, C. D., "Optimal Configurations for Rotating Spacecraft Formations," *Journal of Astronautical Sciences*, Vol. 48, Nos. 2–3, 2000, pp. 225–247.

[10] Campbell, M., Fullmer, R. R., and Hall, C. D., "The ION-F Formation Flying Experiments," *Proceedings of the 2000 AAS/AIAA Space Flight Mechanics Meeting*, Univelt, San Diego, CA, 2000, pp. 135–150.

[11] Naasz, B. J., Karlgaard, C. D., and Hall, C. D., "Application of Several Control Techniques for the Ionospheric Observation Nanosatellite Formation," *Proceedings of the 2002 AAS/AIAA Space Flight Mechanics Meeting*, Univelt, San Diego, CA, 2002, pp. 1063–1080.

[12] Naasz, B. J., "Classical Element Feedback Control for Spacecraft Orbital Maneuvers," M.S. Thesis, Dept. of Aerospace and Ocean Engineering, Virginia Polytechnic Inst. and State Univ., Blacksburg, VA, 2002.

[13] Naasz, B. J., and Hall, C. D., "Classical Element Feedback Control for Spacecraft Orbital Maneuvers," *Journal of Guidance, Control, and Dynamics* (submitted for publication).

[14] Bate, R. R., Mueller, D. D., and White, J. E., *Fundamentals of Astrodynamics*, Dover, New York, 1971, pp. 40, 41.

[15] Dennis, J. E., Jr., and Schnabel, R. B., *Numerical Methods for Unconstrained Optimization and Nonlinear Equations*, Prentice–Hall, Englewood Cliffs, NJ, 1983.

[16] Seydel, R., *From Equilibrium to Chaos: Practical Bifurcation and Stability Analysis*, Elsevier, New York, 1988, Chap. 4.